

HOW DEEP CONVOLUTIONAL NEURAL NETWORKS LOSE SPATIAL INFORMATION WITH TRAINING

Umberto M. Tomasini *, Leonardo Petrini *, Francesco Cagnetta, Matthieu Wyart

Institute of Physics

École Polytechnique Fédérale de Lausanne

name.surname@epfl.ch

ABSTRACT

A central question of machine learning is how deep nets manage to learn tasks in high dimensions. An appealing hypothesis is that they achieve this feat by building a representation of the data where information irrelevant to the task is lost. For image datasets, this view is supported by the observation that after (and not before) training, the neural representation becomes less and less sensitive to diffeomorphisms acting on images as the signal propagates through the net. This loss of sensitivity correlates with performance, and surprisingly correlates with a *gain* of sensitivity to white noise acquired during training. These facts are unexplained, and as we demonstrate still hold when white noise is added to the images of the training set. Here, we (i) show empirically for various architectures that stability to image diffeomorphisms is achieved by spatial pooling in the first half of the net, and by channel pooling in the second half, (ii) introduce a scale-detection task for a simple model of data where pooling is learned during training, which captures all empirical observations above and (iii) compute in this model how stability to diffeomorphisms and noise scale with depth. The scalings are found to depend on the presence of strides in the net architecture. We find that the increased sensitivity to noise is due to the perturbing noise piling up during pooling, after being rectified by ReLU units.

1 INTRODUCTION

Deep learning algorithms can be successfully trained to solve a large variety of tasks (Amodei et al., 2016; Huval et al., 2015; Mnih et al., 2013; Shi et al., 2016; Silver et al., 2017), often revolving around classifying data in high-dimensional spaces. If there was little structure in the data, the learning procedure would be cursed by the dimension of these spaces: achieving good performances would require an astronomical number of training data (Luxburg & Bousquet, 2004). Consequently, real datasets must have a specific internal structure that can be learned with fewer examples. It has been then hypothesized that the effectiveness of deep learning lies in its ability of building ‘good’ representations of this internal structure, which are insensitive to aspects of the data not related to the task (Ansuini et al., 2019; Schwartz-Ziv & Tishby, 2017; Recanatesi et al., 2019), thus effectively reducing the dimensionality of the problem.

In the context of image classification, Bruna & Mallat (2013); Mallat (2016) proposed that neural networks lose irrelevant information by learning representations that are insensitive to small deformations of the input, also called diffeomorphisms. This idea was tested in modern deep networks by Petrini et al. (2021), who introduced the following measures

$$D_f = \frac{\mathbb{E}_{x,\tau} \|f(\tau(x)) - f(x)\|^2}{\mathbb{E}_{x_1,x_2} \|f(x_1) - f(x_2)\|^2}, \quad G_f = \frac{\mathbb{E}_{x,\eta} \|f(x+\eta) - f(x)\|^2}{\mathbb{E}_{x_1,x_2} \|f(x_1) - f(x_2)\|^2}, \quad R_f = \frac{D_f}{G_f}, \quad (1)$$

to probe the sensitivity of a function f —either the output or an internal representation of a trained network—to random diffeomorphisms τ of x (see example in Fig. 1, left), to large white noise perturbations η of magnitude $\|\tau(x) - x\|$, and in relative terms, respectively. Here the inputs images

*Equal contribution.

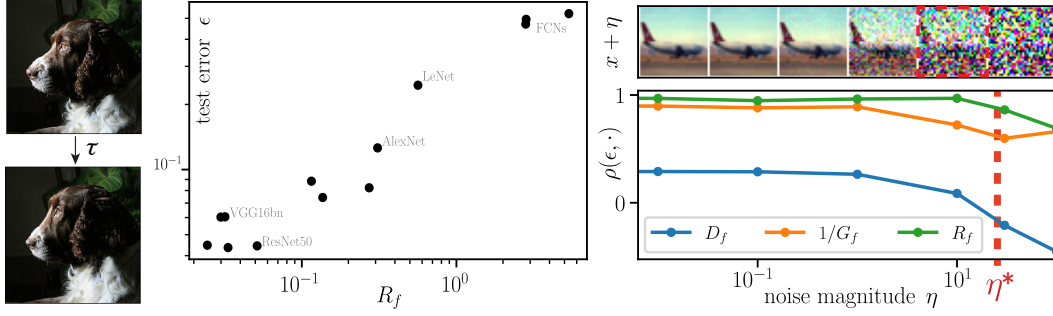


Figure 1: Left: example of a random diffeomorphism τ applied to an image. Center: test error vs relative sensitivity to diffeomorphisms of the predictor for a set of networks trained on CIFAR10, adapted from [Petrini et al. \(2021\)](#). Right: Correlation coefficient between test error ϵ and D_f , G_f and R_f when training different architectures on noisy CIFAR10, $\rho(\epsilon, X) = \text{Cov}(\log \epsilon, \log X) / \sqrt{\text{Var}(\log \epsilon) \text{Var}(\log X)}$. Increasing noise magnitudes are shown on the x -axis and $\eta^* = \mathbb{E}_{\tau, x} \|\tau(x) - x\|^2$ is the one used for the computation of G_f . Samples of a noisy CIFAR10 datum are shown on top. Notice that D_f and particularly R_f are positively correlated with ϵ , whilst G_f is negatively correlated with ϵ . The corresponding scatter plots are in [Fig. 10](#) (appendix).

x , x_1 and x_2 are sampled uniformly from the test set. In particular, the test error of trained networks is correlated with D_f when f is the network output. Less intuitively, the test error is anti-correlated with the sensitivity to white noise G_f . Overall, it is the relative sensitivity R_f which correlates best with the error ([Fig. 1](#), middle). This correlation is learned over training—as it is not seen at initialization—and built up layer by layer ([Petrini et al., 2021](#)). These phenomena are not simply due to benchmark data being noiseless, as they persist when input images are corrupted by some small noise ([Fig. 1](#), right).

Operations that grant insensitivity to diffeomorphisms in a deep network have been identified previously (e.g. [Goodfellow et al. \(2016\)](#), section 9.3, sketched in [Fig. 2](#)). The first, *spatial* pooling, integrates local patches within the image, thus losing the exact location of its features. The second, *channel* pooling, averages the output of different channels, allowing the network to become invariant to any local transformation by properly learning filters that are transformed versions of one another. However, it is not clear whether these operations are actually learned by deep networks and how they conspire in building good representations. Here we tackle this question by unveiling empirically the emergence of spatial and channel pooling, and disentangling their role. Moreover, we introduce an idealized scale-detection task that provides quantitative insight into the role of pooling in *i*) losing spatial information, thus decreasing sensitivity to diffeomorphisms of the inputs, and *ii*) increasing sensitivity to noise. Below is a detailed list of our contributions.

1.1 OUR CONTRIBUTIONS

- We disentangle the role of spatial and channel pooling within deep networks trained on CIFAR10 ([Section 2](#)): spatial pooling tends to be performed in the first part of the network, channel pooling is carried out in the second part.
- We introduce idealized scale-detection tasks ([Section 3](#)) to understand how spatial pooling relates to the sensitivities to diffeomorphisms and noise: data are made of two active pixels and classified according to their distance. We find the same correlations between test error and sensitivities of trained networks as found in [Petrini et al. \(2021\)](#). In addition, the neural networks which perform the best on real data tend to be the best on these tasks.
- We theoretically analyze how simple CNNs, made by stacking convolutional layers with filter size F and stride s , learn these tasks ([Section 4](#)). We find that the trained network performs spatial pooling for most of its layers. We show and verify empirically that the sensitivities D_k and G_k of the k -th hidden layer follow $G_k \sim A_k$ and $D_k \sim A_k^{-\alpha_s}$, where A_k is the effective receptive field size and $\alpha_s = 2$ if there is no stride, $\alpha_s = 1$ otherwise.

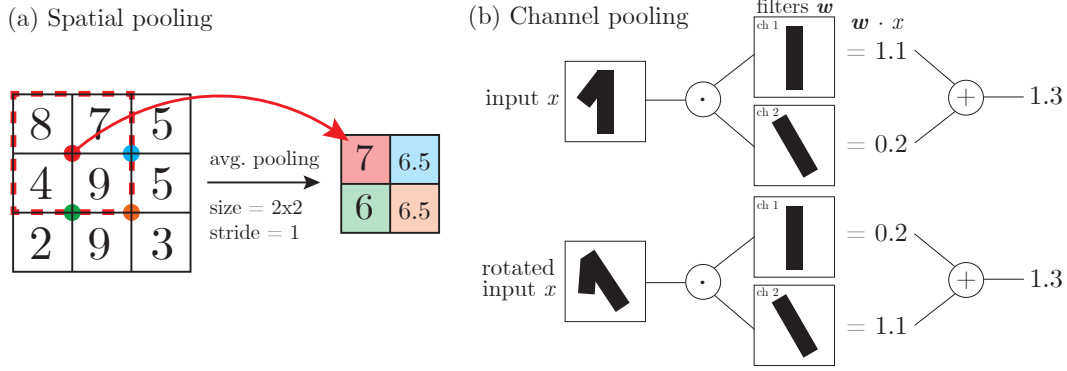


Figure 2: Spatial vs. channel pooling. (a) Spatial average pooling (size 2×2 , stride 1) computed on a representation of size 3×3 . One can notice that nearby pixel variations are smaller after pooling. (b) If the filters of different channels are identical up to e.g. a rotation of angle θ , then, averaging the output of the application of such filters makes the result invariant to input rotations of θ . We refer to this averaging as channel pooling

The code and details for reproducing experiments are available online at github.com/leonardopetrini/relativestability/experiments_ICLR23.md.

1.2 RELATED WORK

In the neuroscience literature, the understanding of the relevance of pooling in building invariant representations dates back to the pioneering work of Hubel & Wiesel (1962). By studying the cat visual cortex, they identified two different kinds of neurons: simple cells responding to e.g. edges at specific angles and complex cells that *pool* the response of simple cells and detect edges regardless of their position or orientation in the receptive field. More recent accounts of the importance of learning invariant representations in the visual cortex can be found in Niyogi et al. (1998); Anselmi et al. (2016); Poggio & Anselmi (2016).

In the context of artificial neural networks, layers jointly performing spatial pooling and strides have been introduced with the early CNNs of Lecun et al. (1998), following the intuition that local averaging and subsampling would reduce the sensitivity to small input shifts. Ruderman et al. (2018) investigated the role of spatial pooling and showed empirically that networks with and without pooling layers converge to similar deformation stability, suggesting that spatial pooling can be learned in deep networks. In our work, we further expand in this direction by jointly studying diffeomorphisms and noise stability and proposing a theory of spatial pooling for a simple task.

The depth-wise loss of irrelevant information in deep networks has been investigated by means of the information bottleneck framework (Shwartz-Ziv & Tishby, 2017; Saxe et al., 2019) and the intrinsic dimension of the networks internal representations (Ansuini et al., 2019; Recanatesi et al., 2019). However, these works do not specify what is the irrelevant information to be disregarded, nor the mechanisms involved in such a process.

The stability of trained networks to noise is extensively studied in the context adversarial robustness (Fawzi & Frossard, 2015; Kanbak et al., 2018; Alcorn et al., 2019; Alaifari et al., 2018; Athalye et al., 2018; Xiao et al., 2018; Engstrom et al., 2019). Notice that our work differs from this literature by the fact that we consider typical perturbations instead of worst-case ones.

2 EMPIRICAL OBSERVATIONS ON REAL DATA

In this section we analyze the parameters of deep CNNs trained on CIFAR10, so as to understand how they build representations insensitive to diffeomorphisms (details of the experiments in App. B). A general diffeomorphism can be represented as a displacement field over the image, which indicates how each pixel moves in the transformation. Locally, this displacement field can be decomposed into a constant term and a linear part: the former corresponds to local translations, the latter to stretchings,

rotations and shears.¹ Invariance to any of these transformations can be achieved via pooling if the internal representations of the network satisfy the following property: different entries of these representations are related to each other by transformations of the input. Once this property holds, adding up related entries results in an invariant representation. More specifically, let us denote with $f_k(x)$ the internal representation of an input x at the k -th layer of the network. The entries of f_k have three indices, one for the channel c and two for the spatial location (i, j) . The relation between f_k and f_{k-1} is the following,

$$[f_k(x)]_{c;i,j} = \phi \left(b_c^k + \sum_{c'=1}^{H_{k-1}} \mathbf{w}_{c,c'}^k \cdot \mathbf{p}_{i,j}([f_{k-1}(x)]_{c'}) \right) \quad \forall c = 1, \dots, H_k, \quad (2)$$

where: H_k denotes the number of channels at the k -th layer; b_c^k and $\mathbf{w}_{c,c'}^k$ the biases and *filters* of the k -th layer; each filter $\mathbf{w}_{c,c'}^k$ is a $F \times F$ matrix with F the filter size; $\mathbf{p}_{i,j}([f_{k-1}(x)]_{c'})$ denotes a $F \times F$ -dimensional patch of $[f_{k-1}(x)]_{c'}$ centered at (i, j) ; ϕ the activation function.

Spatial pooling. Gaining invariance to translations is simple for CNNs thanks to weight sharing: the same convolutional filter $\mathbf{w}_{c,c'}^k$ is applied to all the local patches (i, j) . Thus, entries of f_k corresponding to different spatial locations are related to each other by translations of the input, as exemplified in Fig. 2, panel (a). If entries with different (i, j) are summed up, then the representation will be invariant to translations—this can be achieved by homogeneous filters at the next layer, i.e. all the entries of $\mathbf{w}_{c,c'}^{k+1}$ are the same. We call this operation *spatial pooling* as the sum runs over the spatial indices.

Channel pooling. Relating the different entries of f_k for other transformations of the input requires some additional structure on the filters $\mathbf{w}_{c,c'}^k$. In particular, the $\mathbf{w}_{c,c'}^k$'s must be such that a given transformation of the input x is equivalent to changing the output channel index c in f_k . If this is the case, then the corresponding entries f_k can be summed at the next layer so as to achieve an invariant representation. A two-channel example is shown Fig. 2, panel (b), where the filter of the 2nd channel is built so as to produce the same output as the 1st channel when applied to a rotated input. Since the entries of f_k are being summed over the channel index c , this is called *channel pooling*. Notice that it can be performed by having, at the next layer, filters $\mathbf{w}_{c,c'}^{k+1}$ which are independent of c' .

Disentangling spatial and channel pooling. The relative sensitivity to diffeomorphisms R_k decreases after each layer throughout the network, as shown in Fig. 3. We conclude that spatial and channel pooling are carried out along the whole network. To disentangle their contribution we perform the following experiment: shuffle at random the connections between channels of successive convolutional layers, while keeping the weights unaltered. Channel shuffling amounts to randomly permuting the values of c, c' in Eq. 2. This procedure breaks any learned channel pooling (unless involving all the channels) while not affecting single filters. The values of R_k for deep networks after channel shuffling are reported in Fig. 3 as dashed lines and compared with the original values of R_k in full lines. The two curves overlap for the first part of the networks, implying that channel pooling plays a minor role here, while depart in a second part, where channel pooling has a significant contribution to R_k .

Emergence of spatial pooling after training. Fig. 3 proves that the decrease in relative sensitivity is not caused by channel pooling in the first part of the networks. It suggests that spatial pooling may be at play there. Since spatial pooling can be built by having homogeneous filters, we test for its presence by looking at the frequency content of learned filters $\mathbf{w}_{i,j}^k(t)$ with t the training time. In particular, we consider the average squared projection of filters onto “Fourier modes” $\{\Psi_l\}_{l=1,\dots,F^2}$, taken as the eigenvectors of the discrete Laplace operator on the $F \times F$ filter grid (plotted in Fig. 4, legend). The square projections averaged over channels read

$$\gamma_{k,l}(t) = \frac{1}{H_{k-1}H_k} \sum_{c=1}^{H_k} \sum_{c'=1}^{H_{k-1}} [\Psi_l \cdot \mathbf{w}_{c,c'}^k(t)]^2, \quad (3)$$

¹The displacement field around a pixel (u_0, v_0) is approximated as $\tau(u, v) \simeq \tau(u_0, v_0) + J(u_0, v_0)[u - u_0, v - v_0]^T$, where $\tau(u_0, v_0)$ corresponds to translations and J is the Jacobian matrix of τ whose trace, antisymmetric and symmetric traceless parts correspond to stretchings, rotations and shears, respectively.

and are shown in Fig. 4, 1st row. For a deep network such as VGG11bn (Simonyan & Zisserman, 2015), filters of layers 2 to 5 become low-frequency with training. This observation, together with the fact that R_k shows the same behavior for these layers before and after shuffling channels connections (Fig. 3, red lines), supports that, in this part of the network, spatial pooling has a prominent role in giving relative invariance to diffeomorphisms.

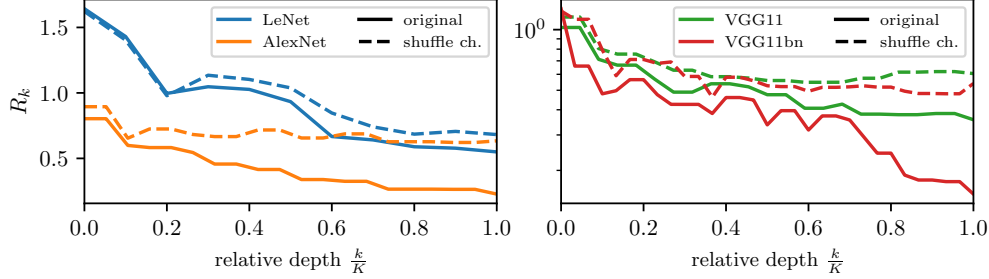


Figure 3: Relative sensitivity R_k as a function of relative depth $\frac{k}{K}$ for networks trained on CIFAR10 (full lines) and when shuffling channels (dashed). K indicates the networks total depth. Earlier (left) and more modern architectures (right) are shown. The two curves start to depart in the second part of the networks, consistently with the hypothesis that channel pooling occurs there.

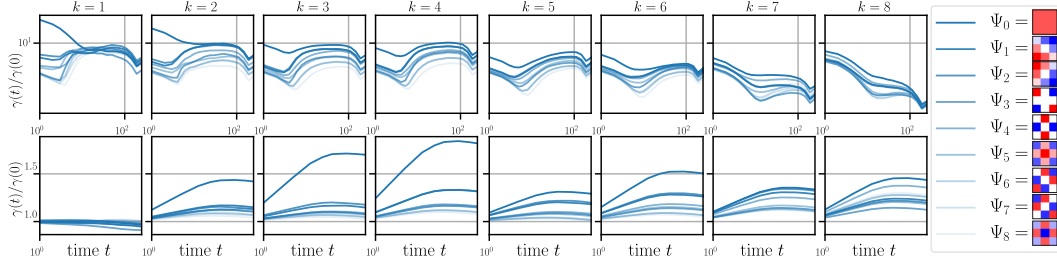


Figure 4: Deep network (VGG11bn) convolutional filters projection on the 9 eigenvectors of the (3×3) -grid Laplacian when training on CIFAR10 (1st row) or the scale-detection task (2nd row): evolution in time, relative to initialization $\gamma_{k,l}(t)/\gamma_{k,l}(0)$. Darker colors correspond to lower frequencies, as reported in the legend. Filters of deeper layers are shown going from left to right. Low-frequency modes are the dominant components in layers 2-5 when training on CIFAR10 and layers 2-4 for scale-detection task 1.

3 SIMPLE SCALE-DETECTION TASKS CAPTURE REAL-DATA OBSERVATIONS

To sum up, the empirical evidence presented in Section 2 indicates that (i) the generalization performance of deep CNNs correlates with their insensitivity to diffeomorphisms and sensitivity to Gaussian noise (Fig. 1); (ii) deep CNNs build their sensitivities layer by layer, first via spatial pooling and then via channel pooling (Fig. 3). We introduce now two idealized scale-detection tasks where the emergence of spatial pooling can be rationalized, and the build-up of insensitivity to diffeomorphisms and sensitivity to Gaussian noise can be understood quantitatively, as we show in Section 4.

Definition of scale-detection tasks. Consider input images x consisting of two active pixels on an empty background.

Task 1: Inputs are classified by comparing the euclidean distance d between the two active pixels and some *characteristic scale* ξ , as in Fig. 5, left. Namely, the label is $y = \text{sign}(\xi - d)$.

Notice that a small diffeomorphism of such images corresponds to a small displacement of the active pixels. By introducing a gap g such that $d \in [\xi - g/2, \xi + g/2]$, task 1 becomes invariant to displacements of size smaller than g . Therefore, we expect that a neural network trained on task 1 will lose any information on the exact location of the active pixels within the image, thus becoming

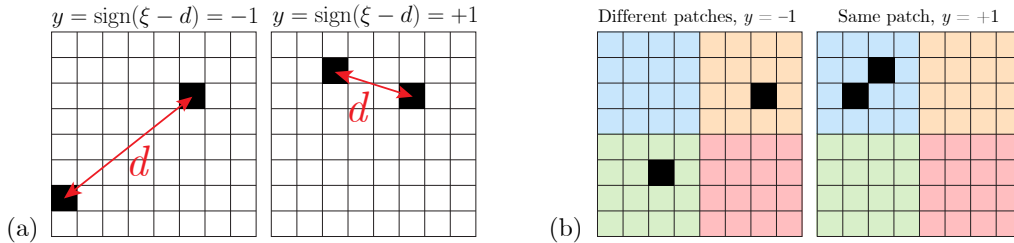


Figure 5: Example inputs for the scale-detection tasks. Task 1 (a): the label depends on whether the euclidean distance d is larger (left) or smaller (right) than the characteristic scale ξ . Task 2 (b): the label depends on whether the active pixels belong to the same patch of size ξ (right) or not (left)—patches are shown in different colors.

insensitive to diffeomorphisms. Spatial pooling is the most direct mean to achieve such insensitivity. In fact, pooling at the scale ξ is equivalent to replacing each pixel with the integral of the image over a patch of size ξ . The result of the integration depends on whether none, one or both the active pixels lie within the pooling window, thus it is still informative of the task.

Task 2: Inputs are partitioned into nonoverlapping patches of size ξ , as in Fig. 5, right. The label y is +1 if the active pixels fall within the same patch, -1 otherwise.

In task 2, the irrelevant information is the location of the pixels within each of the non-overlapping patches. The simplest mean to lose such information requires to couple spatial pooling with a stride of the size of the pooling window itself.

Same phenomenology as in real image datasets. Although these scale-detection tasks are much simpler than standard benchmark datasets, deep networks trained on task 1 display the same phenomenology highlighted in Section 2 for networks trained on CIFAR10. First, the test error is positively correlated with the sensitivity to diffeomorphisms of the network predictor (Fig. 6, left panel) and negatively correlated with its sensitivity to Gaussian noise (middle panel) for a whole range of architectures. As a result, the error correlates well with the relative sensitivity R_f —compare the right panel of Fig. 6 with the left panel of Fig. 1. Secondly, the internal representations of trained networks f_k become progressively insensitive to diffeomorphisms and sensitive to Gaussian noise through the layers, as shown in Fig. 7. Importantly, the curves relating sensitivities to the relative depth remain essentially unaltered if the channels of the networks are shuffled (shown as dashed lines in Fig. 7). We conclude that, on the one hand, the effect of channel pooling is negligible, and, on the other hand, all channels are approximately equal to the mean channel. Finally, direct inspection of the filters (Fig. 4, bottom row) shows that their low-frequency components grow much larger than the others over training, especially for the layers where R_k decreases the most. Filters are thus becoming nearly homogeneous, which means that the convolutional layers become effectively pooling layers.

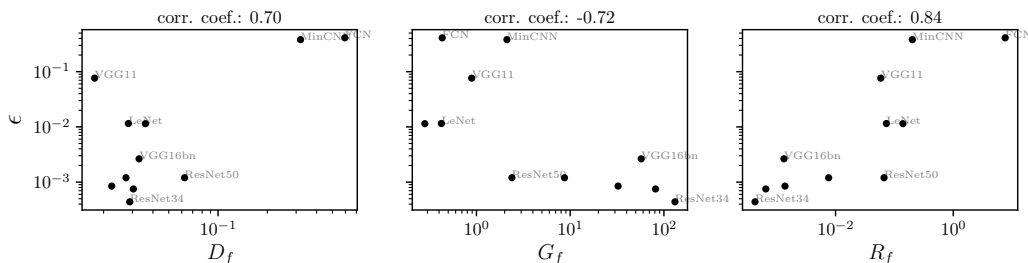


Figure 6: Generalization error ϵ versus sensitivity to diffeomorphisms D_f (left), noise G_f (center) and relative sensitivity R_f (right) for a wide range of architectures trained on scale-detection task 1 (train set size: 1024, image size: 32, $\xi = 14$, $g = 2$). As in real data, ϵ is positively correlated with D_f and negatively correlated with G_f . The correlation is the strongest for the relative measure R_f .

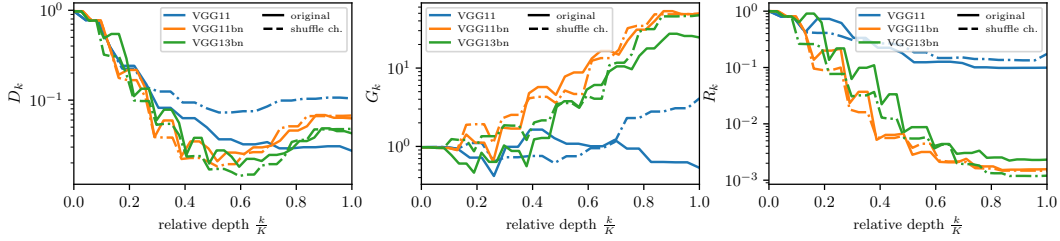


Figure 7: Sensitivities (D_k left, G_k middle and R_k right) of the internal representations vs relative depth for VGG networks trained on scale-detection task 1. Dot-dashed lines show the sensitivities of networks with shuffled channels. All sensitivities are (i) built up mainly in the first part of the network and (ii) approximately insensitive to shuffling of the channels, highlighting that channel pooling plays a negligible role in this task.

4 THEORETICAL ANALYSIS OF SENSITIVITIES IN SCALE-DETECTION TASKS

We now provide a scaling analysis of the sensitivities to diffeomorphisms and noise in the internal representations of simple CNNs trained on the scale-detection tasks of [Section 3](#).

Setup. We consider simple CNNs made by stacking identical convolutional layers with generic filter size F , stride $s = 1$ or F and ReLU activation function $\phi(x) = \max(0, x)$. In particular, we train CNNs with stride 1 on task 1 and CNNs with stride F on task 2. For the sake of simplicity, we consider the one-dimensional version of the scale-detection tasks, but our analysis carries unaltered to the two-dimensional case. Thus, input images are sequences $x = (x_i)_{i=1, \dots, L}$ of L pixels, where $x_i = 0$ for all pixels except two. For the active pixels $x_i = \sqrt{L/2}$, so that all input images have $\|x\|^2 = L$. We will also consider single-pixel data $\delta_j = (\delta_{j,i})_{i=1, \dots, L}$. If the active pixels in x are the i -th and the j -th, then $x = \sqrt{L/2}(\delta_i + \delta_j)$. For each layer k , the internal representation $f_k(x)$ of the trained network is defined as in [Eq. 2](#). The *receptive field* of the k -th layer is the number of input pixels contributing to each component of $f_k(x)$. We define the *effective receptive field* A_k as the typical size of the representation of a single-pixel input, $f_k(\delta_i)$, as illustrated in red in [Fig. 8](#). We denote the sensitivities of the k -th layer representation with a subscript k (D_k for diffeomorphisms, G_k for noise, R_k for relative).

Assumptions. All our results are based on the assumption that the first few layers of the trained network behave effectively as a single channel with a homogeneous filter and no bias. The equivalence of all the channels with their mean is supported by [Fig. 7](#), which shows how shuffling channels does not affect the internal representations. In addition, [Fig. 4](#) (bottom row) shows that the mean filter of the first few layers is nearly homogeneous. We set the homogeneous value of each filter so as to keep the norm of representations constant over layers. Moreover, we recall that a deformation of the input x of our scale-detection tasks can be thought of as a random displacement of each active pixel.

4.1 TASK 1, STRIDE 1

For a CNN with stride 1, under the homogeneous filter assumption, the size of the effective receptive field A_k grows as \sqrt{k} . A detailed proof is presented in [App. A](#) and [Fig. 8](#), left panel, shows an illustration of the process. Intuitively, applying a homogeneous filter to a representation is equivalent to making each pixel diffuse, i.e. distributing its intensity uniformly over a neighborhood of size F . With a single-pixel input δ_i , the effective receptive field of the k -th layer $f_k(\delta_i)$ is equivalent to a k -step diffusion of the pixel, thus it approaches a Gaussian distribution of standard deviation \sqrt{k} centered at i . The size A_k is the standard deviation, thus $A_k \sim \sqrt{k}$.

Sensitivity to diffeomorphisms. Let i and j denote the active pixels locations, so that $x \propto \delta_i + \delta_j$. Since both the elements of the inputs and those of the filters are non-negative, the presence of ReLU nonlinearities is irrelevant and the first few hidden layers are effectively linear layers. Hence the representations are linear in the input, so that $f_k(x) = f_k(\delta_i + \delta_j) = f_k(\delta_i) + f_k(\delta_j)$. In addition,

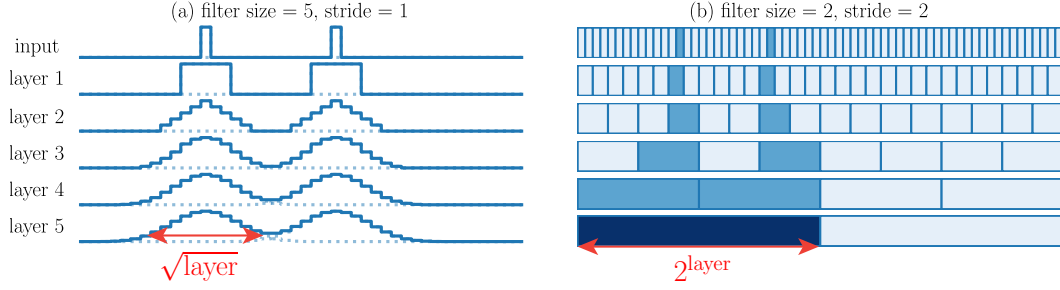


Figure 8: Hidden layers representations of simple CNNs for a scale-detection input for stride $s = 1$ and filter size $F = 5$ (left) and $s = F = 2$ (right) when having homogeneous filters at every layer. The effective receptive field size of the last layer in the two different cases is shown in red. (Left) every active pixel in the input becomes a Gaussian profile whose width increases throughout the network. (Right) every neuron in layer k has activity equal to the number of active pixels which are present in its receptive field of width 2^k . The dark blue in the last layer indicates that there are 2 active pixels in its receptive field, while the lighter blue of the precedent layers indicates that there is just 1.

since the effect of a diffeomorphism is just a 1-pixel translation of the representation irrespective of the original positions of the pixels, the normalized sensitivity D_k can be approximated as follows

$$D_k \sim \frac{\|f_k(\delta_{i+1}) - f_k(\delta_i)\|_2^2}{\|f_k(\delta_i)\|_2^2}. \quad (4)$$

The denominator in Eq. 4 is the squared norm of a Gaussian distribution of width \sqrt{k} , $\|f_k(v_i)\|_2^2 \sim k^{-1/2}$. The numerator compares f_k with a small translation of itself, thus it can be approximated by the squared norm of the derivative of the Gaussian distribution, $\|f_k(\delta_{i+1}) - f_k(\delta_i)\|_2^2 \sim k^{-3/2}$. Consequently, we have

$$D_k \sim k^{-1} \sim A_k^{-2}. \quad (5)$$

Sensitivity to Gaussian noise. To analyze G_k one must take into account the rectifying action of ReLU, which sets all the negative elements of its input to zero. The first ReLU is applied after the first homogeneous filters, thus the zero-mean noise is superimposed on a patch of F active pixels. Outside such a patch, only positive noise terms survive. Within the patch, being summed to a positive background, also negative terms can survive the rectification of ReLU. Nevertheless, if the size of the image is much larger than the filter size, the contribution from active pixels to G_k is negligible and we can approximate the difference between noisy and original representations $f_1(x + \eta) - f_1(x)$ with the rectified noise $\phi(\eta)$. After the first layer, the representations consist of non-negative numbers, thus we can forget again the ReLU and write

$$G_k \sim \frac{\mathbb{E}_\eta \|f_k(\phi(\eta))\|_2^2}{\|f_k(\delta_i)\|_2^2}. \quad (6)$$

Repeated applications of homogeneous filters to the rectified noise $\phi(\eta)$ result again in a diffusion of the signal. Since $\phi(\eta)$ has different independent and identically distributed non-zero entries for different realizations of η , averaging over η is equivalent to considering a homogeneous profile for $f_k(\phi(\eta))$. As a result, the numerator in Eq. 6 is a constant independent of k . The denominator is the same as in Eq. 4, $\|f_k(\delta_i)\|_2^2 \sim k^{-1/2}$, hence

$$G_k \sim k^{1/2} \sim A_k, \quad (7)$$

i.e. the sensitivity to Gaussian noise grows as the size of the effective receptive fields. From the ratio of Eq. 5 and Eq. 7, we get $R_k \sim A_k^{-3}$.

4.2 TASK 2, STRIDE EQUAL FILTER SIZE

When the stride s equals to the filter size F the number of pixels of the internal representations is reduced by a factor F at each layer, thus f_k consists of L/F^k pixels. Meanwhile, the effective size of the receptive fields grows exponentially at the same rate: $A_k = F^k$ (see Fig. 8, left for an illustration).

Sensitivity to diffeomorphisms. For a given layer k , consider a partition of the input image into L/F^k patches. Each pixel of f_k only looks at one such patch and its intensity coincides with the number of active pixels within the patch. As a result, the only diffeomorphisms that change f_k are those which move one of the active pixels from one patch to another. Since active pixels move by 1, this can only occur if one of the active pixels was originally located at the border of a patch, which in turn occurs with probability $\sim 1/F^k$. In addition, the norm $\|f_k(\delta_i)\|_2$ at the denominator does not scale with k , so that

$$D_k \sim F^{-k} \sim A_k^{-1}. \quad (8)$$

Sensitivity to Gaussian noise. Each pixel of f_k looks at a patch of the input of size F^k , thus f_k is affected by the sum of all the noises acting on such patch. Since these noises have been rectified by ReLU, by the Central Limit Theorem the sum scales as the number of summands F^k . Thus, the contribution of each pixel of f_k to the numerator of G_k scales as $(F^k)^2$. As there are L/F^k pixels in f_k , one has

$$G_k \sim (F^k)^2 (L/F^k) \sim F^k \sim A_k. \quad (9)$$

Without rectification, the sum of F^k independent noises would scale as the square root of the number of summands F^k , yielding a constant G_k . We conclude that the rectifying action of ReLU is crucial in building up sensitivity to noise. $R_k \sim A_k^{-2}$ follows from the ratio of Eq. 8 and Eq. 9.

4.3 COMPARING PREDICTIONS WITH EXPERIMENTS

We test our scaling predictions (Eq. 5 to Eq. 9) in Fig. 9, for stride 1 CNNs trained on task 1 and stride F CNNs trained on task 2 in the top and bottom panels, respectively. In order to support the assumption that all channels behave like the mean channel, we plot the sensitivities of the network obtained by averaging all channels per each layer and we observe that they overlap with the original sensitivities in the first part of the network. Further details on the experiments are provided in App. B.

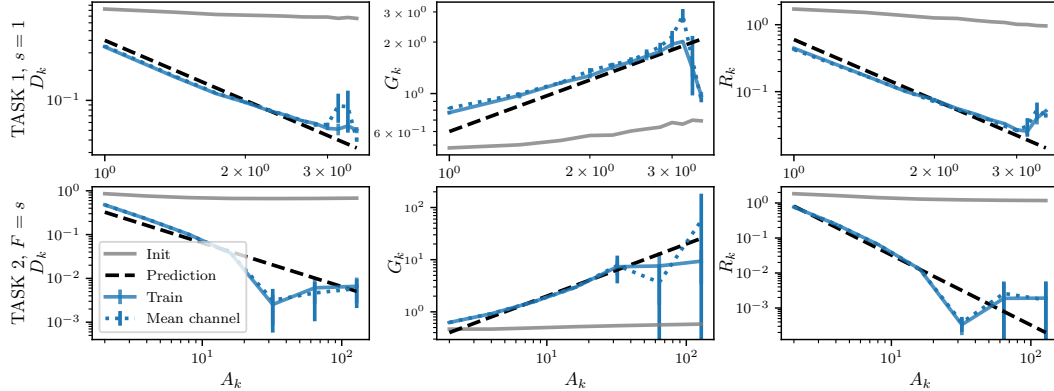


Figure 9: Sensitivities of internal representations f_k of simple CNNs against the k -th layer receptive field size A_k for trained networks (solid blue) and at initialization (solid gray). The top row refers to task 1 with $s = 1$ and $F = 3$; the bottom row to task 2 with $F = s = 2$. For a first large part of the network, the sensitivities obtained by replacing each layer with the mean channel (blue dotted) overlap with the original sensitivities. Predictions of Eq. 5, Eq. 7 for task 1 and Eq. 8, Eq. 9 for task 2 are shown as black dashed lines.

5 CONCLUSION

The meaning of an image often depends on sparse regions of the data, as evidenced by the fact that artists only need a small number of strokes to represent a visual scene. The exact locations of the features determining the image class are flexible, and indeed diffeomorphisms of limited magnitude leave the class unchanged. Here, we have shown that such an invariance is learned in deep networks by performing spatial pooling in the first half of neural networks, and by performing channel pooling in their second half. The most modern architectures learn these pooling operations—as they are not imposed by the architecture—supporting that it is best to let the pooling adapt to the specific task

considered. Interestingly, spatial pooling comes together with an increased sensitivity to random noise in the image, as captured in simple artificial models of data.

It is commonly believed that the best architectures are those that extract the features of the data most relevant for the task. It is likely that the pooling operations studied here, which allow the network to forget the exact locations of these features, are more effective when features are better extracted. This point may be responsible for the observed strong correlations between the network performance and its stability to diffeomorphisms. Designing synthetic models of data that are combinatorial (so as to perform better if features are better extracted) and stable to smooth transformations is very much needed to clarify this relationship, and ultimately understand how deep networks learn high-dimensional tasks with limited data.

ACKNOWLEDGMENTS

We thank Alessandro Favero and Antonio Sclocchi for fruitful discussions. This work was supported by a grant from the Simons Foundation (#454953 Matthieu Wyart).

REFERENCES

- Rima Alaifari, Giovanni S. Alberti, and Tandri Gauksson. ADef: an Iterative Algorithm to Construct Adversarial Deformations. September 2018. URL <https://openreview.net/forum?id=Hk4dFjR5K7>.
- Michael A. Alcorn, Qi Li, Zhitao Gong, Chengfei Wang, Long Mai, Wei-Shinn Ku, and Anh Nguyen. Strike (With) a Pose: Neural Networks Are Easily Fooled by Strange Poses of Familiar Objects. In *2019 IEEE/CVF Conference on Computer Vision and Pattern Recognition (CVPR)*, pp. 4840–4849, Long Beach, CA, USA, June 2019. IEEE. ISBN 978-1-72813-293-8. doi: 10.1109/CVPR.2019.00498. URL <https://ieeexplore.ieee.org/document/8954212/>.
- Dario Amodei, Sundaram Ananthanarayanan, Rishita Anubhai, Jingliang Bai, Eric Battenberg, Carl Case, Jared Casper, Bryan Catanzaro, Qiang Cheng, Guoliang Chen, et al. Deep speech 2: End-to-end speech recognition in english and mandarin. In *International conference on machine learning*, pp. 173–182, 2016.
- Fabio Anselmi, Joel Z. Leibo, Lorenzo Rosasco, Jim Mutch, Andrea Tacchetti, and Tomaso Poggio. Unsupervised learning of invariant representations. *Theoretical Computer Science*, 633:112–121, June 2016. ISSN 0304-3975. doi: 10.1016/j.tcs.2015.06.048. URL <https://www.sciencedirect.com/science/article/pii/S0304397515005587>.
- Alessio Ansuini, Alessandro Laio, Jakob H Macke, and Davide Zoccolan. Intrinsic dimension of data representations in deep neural networks. In *Advances in Neural Information Processing Systems*, pp. 6111–6122, 2019.
- Anish Athalye, Logan Engstrom, Andrew Ilyas, and Kevin Kwok. Synthesizing Robust Adversarial Examples. In *International Conference on Machine Learning*, pp. 284–293. PMLR, July 2018. URL <http://proceedings.mlr.press/v80/athalye18b.html>. ISSN: 2640-3498.
- Joan Bruna and Stéphane Mallat. Invariant scattering convolution networks. *IEEE transactions on pattern analysis and machine intelligence*, 35(8):1872–1886, 2013.
- Logan Engstrom, Brandon Tran, Dimitris Tsipras, Ludwig Schmidt, and Aleksander Madry. Exploring the Landscape of Spatial Robustness. In *International Conference on Machine Learning*, pp. 1802–1811. PMLR, May 2019. URL <http://proceedings.mlr.press/v97/engstrom19a.html>. ISSN: 2640-3498.
- Alhussein Fawzi and Pascal Frossard. Manitest: Are classifiers really invariant? In *Proceedings of the British Machine Vision Conference 2015*, pp. 106.1–106.13, Swansea, 2015. British Machine Vision Association. ISBN 978-1-901725-53-7. doi: 10.5244/C.29.106. URL <http://www.bmva.org/bmvc/2015/papers/paper106/index.html>.
- Ian Goodfellow, Yoshua Bengio, and Aaron Courville. *Deep Learning*. The MIT Press, Cambridge, Massachusetts, November 2016. ISBN 978-0-262-03561-3.

-
- D. H. Hubel and T. N. Wiesel. Receptive fields, binocular interaction and functional architecture in the cat's visual cortex. *The Journal of Physiology*, 160(1):106–154.2, January 1962. ISSN 0022-3751. URL <https://www.ncbi.nlm.nih.gov/pmc/articles/PMC1359523/>.
- Brody Huval, Tao Wang, Sameep Tandon, Jeff Kiske, Will Song, Joel Pazhayampallil, Mykhaylo Andriluka, Pranav Rajpurkar, Toki Migimatsu, Royce Cheng-Yue, et al. An empirical evaluation of deep learning on highway driving. *arXiv preprint arXiv:1504.01716*, 2015.
- Can Kanbak, Seyed-Mohsen Moosavi-Dezfooli, and Pascal Frossard. Geometric Robustness of Deep Networks: Analysis and Improvement. In *2018 IEEE/CVF Conference on Computer Vision and Pattern Recognition*, pp. 4441–4449, Salt Lake City, UT, June 2018. IEEE. ISBN 978-1-5386-6420-9. doi: 10.1109/CVPR.2018.00467. URL <https://ieeexplore.ieee.org/document/8578565/>.
- Y. Lecun, L. Bottou, Y. Bengio, and P. Haffner. Gradient-based learning applied to document recognition. *Proceedings of the IEEE*, 86(11):2278–2324, November 1998. ISSN 1558-2256. doi: 10.1109/5.726791. Conference Name: Proceedings of the IEEE.
- Ulrike von Luxburg and Olivier Bousquet. Distance-based classification with lipschitz functions. *Journal of Machine Learning Research*, 5(Jun):669–695, 2004.
- Stéphane Mallat. Understanding deep convolutional networks. *Philosophical Transactions of the Royal Society A: Mathematical, Physical and Engineering Sciences*, 374(2065):20150203, 2016.
- Volodymyr Mnih, Koray Kavukcuoglu, David Silver, Alex Graves, Ioannis Antonoglou, Daan Wierstra, and Martin Riedmiller. Playing atari with deep reinforcement learning. *arXiv preprint arXiv:1312.5602*, 2013.
- P. Niyogi, F. Girosi, and T. Poggio. Incorporating prior information in machine learning by creating virtual examples. *Proceedings of the IEEE*, 86(11):2196–2209, November 1998. ISSN 1558-2256. doi: 10.1109/5.726787. Conference Name: Proceedings of the IEEE.
- Leonardo Petrini, Alessandro Favero, Mario Geiger, and Matthieu Wyart. Relative stability toward diffeomorphisms indicates performance in deep nets. In *Advances in Neural Information Processing Systems*, volume 34, pp. 8727–8739. Curran Associates, Inc., 2021. URL <https://proceedings.neurips.cc/paper/2021/hash/497476fe61816251905e8baafdf54c23-Abstract.html>.
- Tomaso A. Poggio and Fabio Anselmi. *Visual Cortex and Deep Networks: Learning Invariant Representations*. September 2016. doi: 10.7551/mitpress/10177.001.0001. URL <https://direct.mit.edu/books/book/4088/Visual-Cortex-and-Deep-NetworksLearning-Invariant>.
- Stefano Recanatesi, Matthew Farrell, Madhu Advani, Timothy Moore, Guillaume Lajoie, and Eric Shea-Brown. Dimensionality compression and expansion in deep neural networks. *arXiv preprint arXiv:1906.00443*, 2019.
- Hannes Risken. *The Fokker-Planck Equation Springer Series in Synergetics*. 1996.
- Avraham Ruderman, Neil C. Rabinowitz, Ari S. Morcos, and Daniel Zoran. Pooling is neither necessary nor sufficient for appropriate deformation stability in CNNs. *arXiv:1804.04438 [cs, stat]*, May 2018. URL <http://arxiv.org/abs/1804.04438>. arXiv: 1804.04438.
- Laurent Saloff-Coste and Pierre Bremaud. Markov chains: Gibbs fields, monte carlo simulation, and queues. *Journal of the American Statistical Association*, 95, 2000. ISSN 01621459. doi: 10.2307/2669802.
- Andrew M Saxe, Yamini Bansal, Joel Dapello, Madhu Advani, Artemy Kolchinsky, Brendan D Tracey, and David D Cox. On the information bottleneck theory of deep learning. *Journal of Statistical Mechanics: Theory and Experiment*, 2019(12):124020, 2019.
- Baoguang Shi, Xiang Bai, and Cong Yao. An end-to-end trainable neural network for image-based sequence recognition and its application to scene text recognition. *IEEE transactions on pattern analysis and machine intelligence*, 39(11):2298–2304, 2016.

Ravid Shwartz-Ziv and Naftali Tishby. Opening the black box of deep neural networks via information. *arXiv preprint arXiv:1703.00810*, 2017.

David Silver, Julian Schrittwieser, Karen Simonyan, Ioannis Antonoglou, Aja Huang, Arthur Guez, Thomas Hubert, Lucas Baker, Matthew Lai, Adrian Bolton, et al. Mastering the game of go without human knowledge. *nature*, 550(7676):354–359, 2017.

K. Simonyan and Andrew Zisserman. Very Deep Convolutional Networks for Large-Scale Image Recognition. *ICLR*, 2015.

Chaowei Xiao, Jun-Yan Zhu, Bo Li, Warren He, Mingyan Liu, and Dawn Song. Spatially Transformed Adversarial Examples. February 2018. URL <https://openreview.net/forum?id=HyydRMZC->.

APPENDIX

A TASK 1, STRIDE 1: PROOFS

In [Section 4.1](#) we study a simple CNN with stride $s = 1$ and filter size F trained on scale-detection task 1 and postulated that this network displays a one-channel solution with homogeneous filter $[1/F, \dots, 1/F]$ and no biases. We can understand the representation $f_k(x)$ at layer k of an input datum x by using single-pixel inputs δ_i . Let us recall that these inputs have all components to 0 except the i -th, set to 1. Then, we have that a general datum x is given by $x \propto (\delta_i + \delta_j)$, where i and j are the locations of the active pixel in x . We have argued in the main text that the representation $f_k(\delta_i)$ is a Gaussian distribution with width \sqrt{k} . In this Appendix we prove this statement.

First, we observe that in this solution, since both the elements of the filters and those of the inputs are non-negative, the networks behaves effectively as a linear operator. In particular, each layer corresponds to the application of a $L \times L$ circulant matrix M , which is obtained by stacking all the L shifts of the following row vector,

$$\underbrace{[1, 1, \dots, 1]_F}_{F} \underbrace{[0, 0, 0, \dots, 0]_{L-F}}_{L-F}. \quad (10)$$

with periodic boundary conditions. The first row of such a matrix is fixed as follows. If F is odd the patch of size F is centered on the first entry of the first row, while if F is even we choose to have $(F/2)$ ones at left of the first entry and $(F/2) - 1$ at its right. The output f_k of the layer k is then the following: $f_k(\delta_i) = M^k \delta_i$.

Proposition A.1 *Let's consider the $L \times L$ matrix M and a given L vector δ_i , as defined above. For odd $F \geq 3$, in the limit of large width L and large depth k , we have that*

$$(M^k)_{ab} \delta_i = \frac{1}{2\sqrt{\pi}\sqrt{D^{(1)}}\sqrt{k}} e^{-\frac{(a-i)^2}{4D^{(1)}k}}, \quad D^{(1)} = \frac{1}{12F}(F-1)^3, \quad (11)$$

while for even F :

$$(M^k)_{ab} \delta_i = \frac{1}{2\sqrt{\pi}\sqrt{D^{(2)}}\sqrt{k}} e^{-\frac{(v^{(2)}k+a-i)^2}{4D^{(2)}k}}, \quad D^{(2)} = \frac{1}{12F}(F^3 - 3F^2 + 6F - 4), \quad (12)$$

with $v^{(2)} = (1 - F)/(2F)$.

Proof: The matrix M can be seen as the stochastic matrix of a Markov process, where at each step the random walker has uniform probability $1/F$ to move in a patch of width F around itself. We write the following recursion relation for odd F ,

$$p_{a,i}^{(k+1)} = \frac{1}{F} \left(p_{a-(F-1)/2,i}^{(k)} + \dots + p_{a,i}^{(k)} + \dots + p_{a+(F-1)/2,i}^{(k)} \right), \quad (13)$$

and even F ,

$$p_{a,i}^{(k+1)} = \frac{1}{F} \left(p_{a-F/2,i}^{(k)} + \dots + p_{a,i}^{(k)} + \dots + p_{a+(F/2-1),i}^{(k)} \right). \quad (14)$$

In any of these two cases, this is the so-called master equation of the random walk ([Risken, 1996](#)). In the limit of large image width $L \gg 1$ and large depth $k \gg 1$, we can write the related equation for the continuous process $p_i(a, k)$, which is called Fokker-Planck equation in physics and chemistry ([Risken, 1996](#)) or forward Kolmogorov equation in mathematics ([Saloff-Coste & Bremaud, 2000](#)),

$$\partial_k p_{a,i}^{(k)} = v \partial_a p_{a,i}^{(k)} + D \partial_a^2 p_{a,i}^{(k)}, \quad (15)$$

where the drift coefficient v and the diffusion coefficient D are defined in terms of the probability distribution $W_i(x)$ of having a jump x starting from the location i

$$a = \int dx W_i(x) x, \quad D = \int dx W_i(x) x^2. \quad (16)$$

In our case we have $W_i(x) = 1/F$ for $x \in [i - (F-1)/2, i + (F-1)/2]$ for odd F and $x \in [i - F/2, i + F/2 - 1]$ for even F , yielding the solutions for the related Fokker-Planck equations reported in [Eq. 11](#) and [Eq. 12](#). \square

B EXPERIMENTAL SETUP

All experiments are performed in PyTorch. The code with the instructions on how to reproduce experiments are found here: github.com/leonardopetrini/relativestability/experiments_ICLR23.md.

B.1 DEEP NETWORKS TRAINING

In this section, we describe the experimental setup for the training of the deep networks deployed in Sections 1, 2 and 3.

For CIFAR10, fully connected networks are trained with the ADAM optimizer and learning rate = 0.1 while for CNNs SGD, learning rate = 0.1 and momentum = 0.9. In the latter case, the learning rate follows a cosine annealing scheduling. In all cases, the networks are trained on the cross-entropy loss, with a batch size of 128 and for 250 epochs. Early stopping at the best validation error is performed for selecting the networks to study. During training, we employ standard data augmentation consisting of random translations and horizontal flips of the input images. On the scale-detection task, we perform SGD on the hinge loss and halve the learning rate to 0.05. All results are averaged when training on 5 or more different networks initializations.

B.2 SIMPLE CNNs TRAINING

In this section we present the experimental setup for the training of simple CNNs introduced in Section 4, whose sensitivities to diffeomorphisms and Gaussian noise are shown in Fig. 9.

To learn task 1 we use CNNs with stride $s = 1$ and filter size $F = 3$. The width of the CNN is fixed to 1000 channels, while the depth to 12 layers. We use the Scale-Detection task in the version of Fig. 5 (b), with $\xi = 11$ and gap $g = 4$ and image size $L = 32$. For the training, we use $P = 48$ training points and Stochastic Gradient Descent (SGD) with learning rate 0.01 and batch size 8. We use weight decay for the L_2 norm of the filters weights with ridge 0.01. We stop the training after 500 times the interpolation time, which is the time required by the network to reach zero interpolation error of the training set. The goal of this procedure is to reach the solution with minimal norm. The generalization error of the trained CNNs is exactly zero: they learn spatial pooling perfectly. We show the sensitivities of the trained CNNs, averaged over 4 seeds, in the top panels of Fig. 9, where we also successfully test the predictions (Eq. 5, Eq. 7). We remark that to compute G_k we inserted Gaussian noise with already the ReLU applied on, since we observe that without it we would see a pre-asymptotic behaviour for G_k with respect to A_k .

Task 2 is learned using CNNs with stride equal to filter size $s = F = 2$. For the dataset, we use the block-wise version of the Scale-Detection task shown in Fig. 5 (c), fixing $\xi = 2^5$ and $L = 2^7$. We use 7 layers and 1000 channels for the CNNs. The training is performed using SGD and weight decay with the same parameters as in task 1, with $P = 2^{10}$ training points. In the bottom panels of Fig. 9 we show that the predictions (Eq. 8, Eq. 9) capture the experimental results, averaged over 10 seeds.

C ADDITIONAL FIGURES

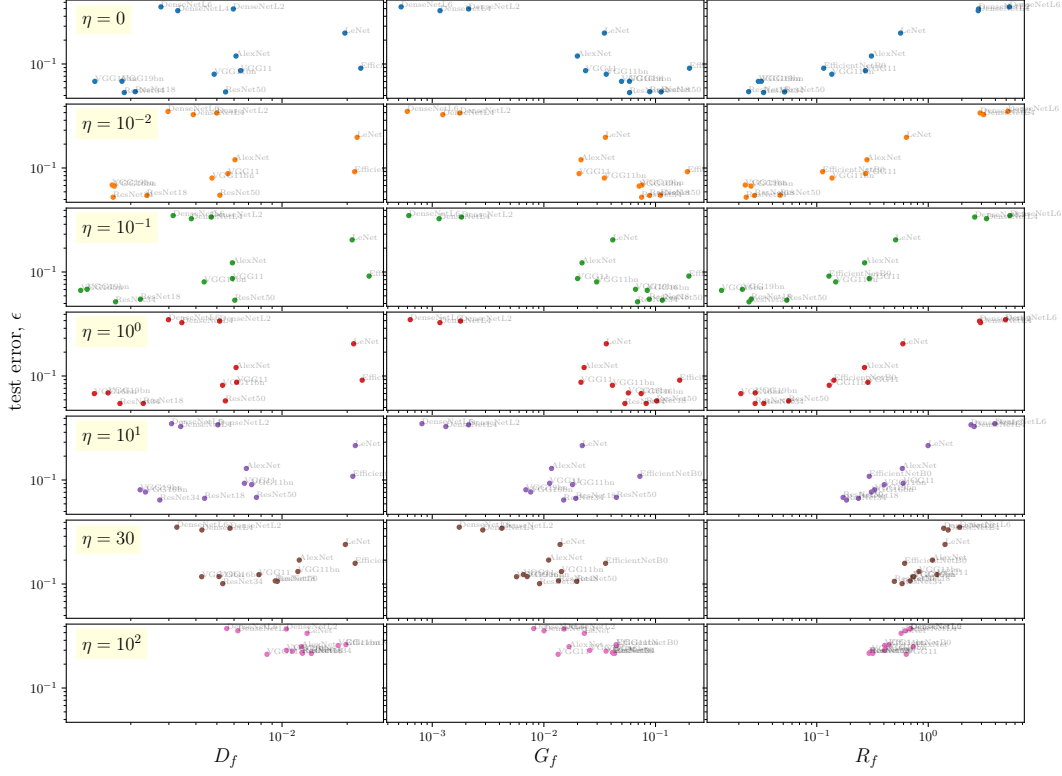


Figure 10: Test error vs. sensitivities (columns) when training on noisy CIFAR10. The different rows correspond to increasing noise magnitude η . Different points correspond to networks architectures, see gray labels. The content of this figure is also represented in compact form in Fig. 1, right.